

Fast square-oscillations in semiconductor VCSELs with delayed orthogonal polarization feedback

Tao Wang¹, Zhicong Tu¹, Yixing Ma¹, Yiheng Li¹, Zhibo Li¹, Fan Qin¹, Stephane Barland², and Shuiying Xiang¹

¹State Key Laboratory of Integrated Service Networks, Xidian University, Xi'an 710071, China and

²Université Côte d'Azur, Institute de Physique de Nice, UMR 7010 CNRS, Nice, 06200, France

(Dated: December 16, 2024)

We present an experimental study on the generation of self-sustained and fast square oscillations from the TE mode of semiconductor VCSELs with delayed orthogonal polarization feedback. We find that the low frequency switching originates from the rotation of the TE and TM modes facilitated by a long time delay, but the fast oscillations are anchored to the frequency beating between the TE and TM modes and are modified by a half-wavelength ($\lambda/2$) plate. A comprehensive analysis of the evolution of the nonlinear dynamics is conducted and the related mechanism is discussed. Our study not only deepens our comprehension of laser nonlinear dynamics but also offers an all-optical approach for producing specialized signals, which could be instrumental in applications such as optical communications and photonic computing.

PACS numbers:

INTRODUCTION

Semiconductor lasers, in particular Vertical Cavity Surface Emitting Lasers (VCSELs), submitted to external-cavity optical feedback are considered as ideal systems for studying nonlinear dynamics. The interplay between different frequency oscillations, such as the relaxation oscillation frequency, the mode beat frequency, the mode switching frequency, the external-cavity frequency, and the current modulation frequency, can generate rich dynamics including chaos, periodic oscillations, and regular pulse trains can be generated [1–3]. Those dynamical behaviors possess various potential applications in secure optical communications [4, 5], high speed random bit generators [6, 7], chaotic radar [8, 9], and photonic spiking neural networks [10, 11]. Thus, the investigation on the nonlinear system of semiconductor lasers with external optical feedback have attracted increasing interest and research attention, not merely from a fundamental physics perspective, but also for their new potentials on enabling practical applications.

One particular example of a dynamical regime that can arise through external feedback is square-wave (SW) switching. Square-wave oscillations are needed as clocks in signal processing and optical communications [12, 13]. Using the semiconductor lasers with optical feedback, SW modulation of emitted power in each polarization channel has been investigated in edge-emitting lasers (EELs) through crossed-polarization re-injection (XPR) [14, 15]. In such a system, the optical feedback from an external cavity couples asymmetrically from the TE mode to the non-lasing, orthogonal TM mode, resulting in square-wave oscillations with a period approximately twice the delay introduced by the external feedback path. Typically, the square-wave self-modulation exhibits a duty cycle of approximately 50%. Then, in the system of two edge-emitting lasers

(EELs) coupled through polarization-rotated feedback, asymmetric duty cycles with overall period close to the feedback roundtrip time have been observed [16, 17].

The investigation of SWs generation has also extended to VCSELs. Notably, VCSELs usually emit linearly polarized light due to the symmetry of their gain medium and their inherent material anisotropy [18, 19]. The losses associated with the orthogonal mode are significantly lower compared to those in edge-emitting lasers (EELs) [20]. Polarization self-modulation can be induced when polarization-rotated feedback is employed, facilitating the switching between the two orthogonal linearly polarized modes, resulting in the generation of SWs [21, 22]. Besides, the period of such SWs is also close to twice the re-injection delay. More robust SWs can be obtained by additionally exposing the VCSELs to polarization selective optical feedback [23]. In this configuration, two different setups have been considered: 1) each of the orthogonal polarization is reinjected into the laser after being rotated by 90° ; 2) one polarization is filtered out while the other is turned by 90° [24]. In Vertical External Cavity Lasers with optical injection, more complex temporal patterns have been observed, including temporal localized states [25].

In this work, we report on our observations of square-wave (SW) polarization switching and fast oscillations using a semiconductor VCSEL with delayed orthogonal-polarization feedback. The VCSEL operates in two linear polarization modes: TE and TM modes, which exhibit large threshold difference. Within the investigation region, the TE mode dominates the lasing behavior, while the TM mode is significantly suppressed. An external ring cavity containing a $\lambda/2$ wave plate is employed to rotate the polarizations of both modes. We conduct a comprehensive investigation of the evolution of SWs as functions of pump current and the phase modification through the $\lambda/2$ wave plate within the

external cavity. Our findings reveal that both the amplitude and duration of the SW can be adjusted by modifying these parameters. We also focus on the fast polarization dynamics which accompanies the SW and show that the non-zero part of the SW is in fact dominated by very fast oscillations which in general maintain very well defined phase relation from one round-trip to the next. This research offers an alternative approach for generating SWs and fast polarization dynamics, which are significant for applications in optical communications and optical computing [24, 26].

EXPERIMENTAL SETUP

Fig. 1 displays the schematic of the experimental design, where a thermally stabilized semiconductor VCSEL (Thorlabs L850VH1, $\lambda = 850$ nm at $T = 25^\circ\text{C}$) is employed as the light source. The laser is operated in a single longitudinal mode and single transverse mode, and is driven by a low-noise current source (Thorlabs LDC205C). The temperature is stabilized at 25°C by a temperature controller (Thorlabs TED200C), better than 0.001°C . The collimated laser light initially passes through a beam splitter (BS, 50:50), causing the beam to be divided into two equal-intensity beams. One beam goes to an amplified fast detector (10 GHz bandwidth) after passing through an optical isolator, and the temporal signals are monitored by a 20 GHz oscilloscope (Tektronix DSA72004, sampling rate is 50 GHz). Meanwhile, the other one is directed towards an external ring cavity. Upon passing through a polarized beam splitter (PBS), the TE and TM modes are separated and circulate in opposing directions within the external cavity. After traversing a $\lambda/2$ plate, they undergo a 90° rotation. The total feedback length is 0.9 m, which corresponds to a round-trip time of 12 ns. We adjust the optical isolator's input polarizer such that we detect the TE mode dynamics.

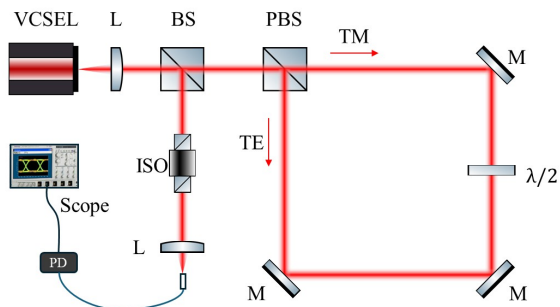


FIG. 1: Experimental setup: L, optical lens; BS, beam splitter; PBS, polarized beam splitter; M, mirror; $\lambda/2$, half-wave plate; ISO, optical isolator; PD, amplified high-speed photodetector; Osc., oscilloscope.

RESULTS AND DISCUSSIONS

Fig. 2a shows the input-output function curves of the TE mode (red) and the TM mode (black) as a function of pump current. The TE mode exhibits a significantly lower threshold than the TM mode, specifically $P_{th}^{TE} = 1.48$ mA and $P_{th}^{TM} = 5.20$ mA = $3.51P_{th}^{TE}$. Within the range of $P_{th}^{TE} < P < P_{th}^{TM}$, the output power of the TE mode increases linearly with the input current. However, the TM mode is strongly suppressed, the signal is approximately close to zero. When $P > P_{th}^{TM}$, the output power of the TM mode starts to increase. In this current region, fluctuations at low frequency are observed in the RF spectrum of both the TM and TE modes suggesting complex polarization dynamics taking place. Fig. 2b shows the radio frequency (RF) spectrum obtained from the free running laser at $P = 5.62$ mA = $3.8P_{th}^{TE}$. For specific orientation of the isolator's input polarizer, we observe three distinct peaks located at 4.8 GHz, 7.5 GHz, and 9.8 GHz, respectively. The inset shows the relaxation oscillation frequency of the TE mode with current, and the corresponding square root fit. After a close inspection of the curve for the frequency at $P = 3.8P_{th}^{TE}$, we interpret the peak at 9.8 GHz as the relaxation oscillation frequency of the TE mode and the peak at 4.8 GHz as the relaxation oscillations of the TM mode. The central peak at 7.5 GHz can be interpreted as the beating note between TE and TM and therefore corresponds to the VCSEL's birefringence.

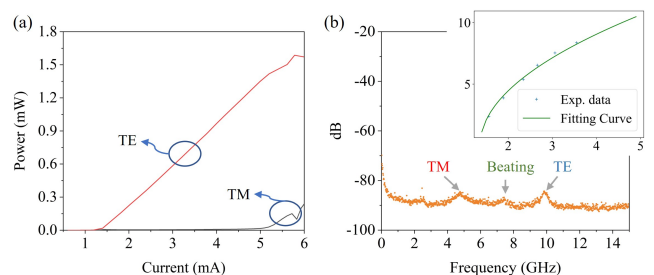


FIG. 2: Lasing function curves and typical RF spectrum of the free running VCSEL: (a) input-output function curves as a function of pump current. The red curve indicates the TE mode, and the black curve denotes the TM mode; (b) typical RF spectrum obtained from the electrical spectrum analyzer (ESA) characterization after balancing the polarization. Inset, relaxation oscillation frequency of the free running laser's TE mode as a function of the pump current.

Fig. 3a plots the temporal waveform within one period $\tau = \tau_1 + \tau_2$, corresponding to one round-trip. It shows two distinct states that alternate in time: one is the steady state accompanied by background noise, lasting $\tau_1 = 7.0$ ns, while the second state is characterized by fast oscillations, with a duration of $\tau_2 = 5.0$ ns. It is important to note that the noise waveform is attributed to the detection noise. Therefore, given that the TM

mode operates below the threshold with nearly zero intensity, the switching occurs between a steady state for the TM mode and fast oscillations associated with the TE mode.

Fig. 3b displays the corresponding RF spectrum obtained after performing a Fourier transform on the temporal signal sequence. It is clear that a distinct central peak is located at $f_R = 7.6$ GHz, indicating the fast oscillation frequency of the TE mode, which is consistent with the birefringence measured in the free-running laser. In addition, we observe a series of side modes that contribute to a comb-like structure in the spectrum, which come from the longitudinal modes of the external cavity. Upon closer inspection, we note that the spacing between the side modes is consistently measured at 80 MHz. This specific spacing can be interpreted as being equivalent to twice the feedback delay. The presence of these side modes suggests that the laser system is exhibiting complex interactions that stem from the feedback loop dynamics.

Fig. 3c illustrates the spatio-temporal diagram of the typical square-oscillations from the TE mode when the laser is operated at $2.86P_{th}^{TE}$, with the angle of the $\lambda/2$ plate at 96° . In this representation of a delayed feedback system's dynamics [27], the x -axis represents the time within one round-trip, which is equivalent to twice the feedback delay time, while the y -axis indicates the number of round trips. The diagram shows a near vertical straight banded structure which indicates the robust square oscillations resonant with the chosen comoving reference frame of 12 ns. Fig. 3d provides an in-depth view of the fast oscillation region, as indicated by the orange square in Fig. 3c. It is evident that a regular lattice structure is formed by the peaks of the temporal oscillations. The time interval between adjacent peaks is approximately $t_{in} = 0.13$ ns. The stability of this structure indicates a well defined phase relation is preserved from roundtrip to roundtrip. However, the clear slope of this stripe pattern indicates that this fast dynamics is not stationary in the SW reference frame.

To further study the formation of the square wave, we plot the dynamics as a function of pump current, utilizing a fixed $\lambda/2$ plate set at 96° , as shown in Fig. 4. At low pump currents, the laser operates stably, producing a constant intensity output predominantly in the TE mode. The low-level feedback mechanism maintains this stability, ensuring that the laser does not deviate from its operational parameters. As we increase the pump current to $2.64P_{th}^{TE}$, we observe undamped oscillations in the output with frequency peaks around 7.5 GHz and 7.8 GHz (as depicted in Fig. 4d). The dominant peaks correlate with the observed oscillation frequencies, while weaker modes appear at 15.6 GHz, suggesting the higher order harmonics.

When the pump current reaches $2.86P_{th}^{TE}$, we observe robust square fast oscillations characterized by a duration

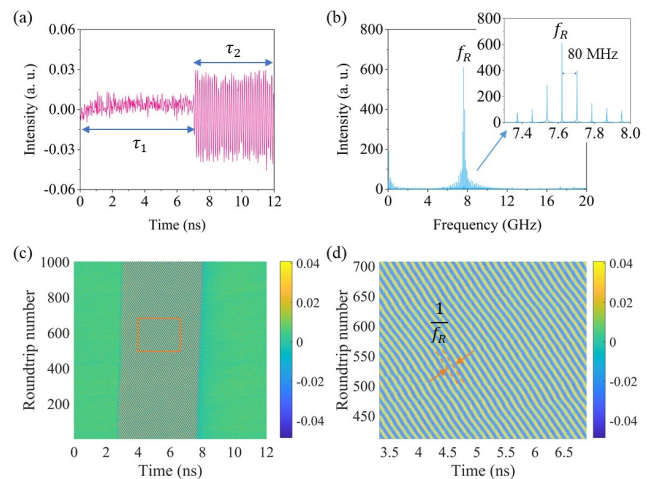


FIG. 3: Square wave characterization: (a) spatiotemporal diagram of the square wave dynamics when the pump current is 4.24 mA and the $\lambda/2$ is 96° ; (b) the highlighted structure, which is outlined by the orange square in (a); (c) temporal dynamics within one period; (d) RF spectrum corresponding to the temporal signal. Inset, enlarged central frequency region.

of $\tau_2 = 6.68$ ns and a steady interval of $\tau_1 = 5.40$ ns (illustrated in Fig. 4b). The overall period of this temporal structure is still $\tau_1 + \tau_2 = 12.08$ ns, corresponding to twice the delay feedback time. The RF spectrum at this stage shows a dominant peak at 7.6 GHz, with satellite peaks which correspond to the external cavity mode spacing (Fig. 4e). Accordingly, the low frequency region of the power spectrum shows peaks separated by 80 MHz with a strong dominance of the odd harmonics as expected for a square wave signal (as shown in the inset of Fig. 4e).

Increasing the pump current further to $3.24P_{th}^{TE}$ results in a notable shift in dynamics. The system exhibits decreased intensity square oscillations, characterized by an asymmetric square wave profile (shown in Fig. 4c). The duration of the oscillations broadens to $\tau_2 = 8.13$ ns, while the steady interval shortens to $\tau_1 = 3.87$ ns. This shift corresponds with a reduced intensity in the RF spectrum and a central frequency shift to higher values, indicating a change in the relaxation oscillation frequency of the TE mode. Additionally, the prominence of low-frequency harmonics suggests a transition towards chaotic behavior within the laser system.

Next, we investigate the influence of the $\lambda/2$ plate on the temporal dynamics of the laser output. Laser systems often exhibit complex dynamics characterized by the interplay of TE and TM modes. The introduction of optical elements, such as a $\lambda/2$ plate, allows for manipulation of these modes. The $\lambda/2$ plate rotates the polarization of incoming light, effectively altering the phase and amplitude of the TE and TM modes. Therefore, We maintained a constant pump current at

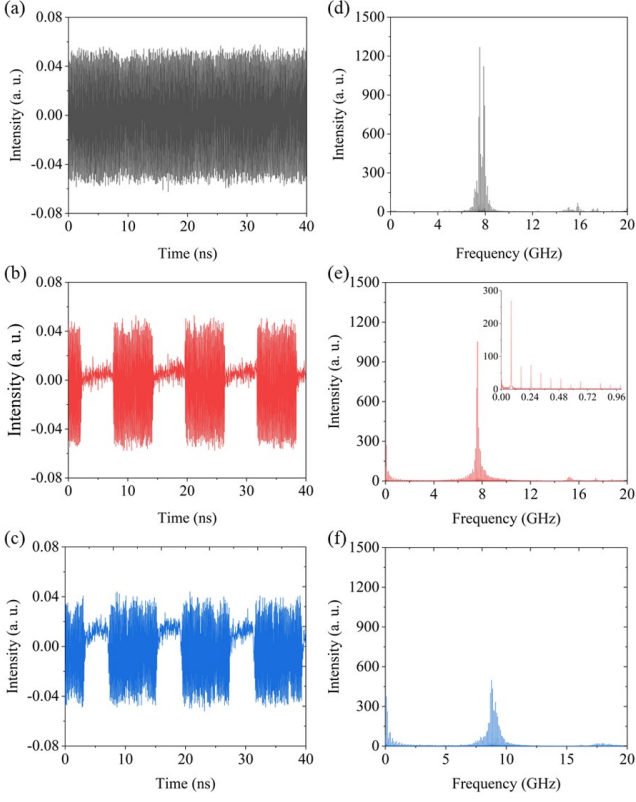


FIG. 4: Temporal dynamics and the corresponding RF spectra of the TE mode for different pump currents: (a) and (d), $2.64P_{th}^{TE}$; (b) and (e), $2.86P_{th}^{TE}$; (c) and (f) $3.24P_{th}^{TE}$.

$2.87P_{th}^{TE}$ and varied the angle of the $\lambda/2$ plate. In Fig. 5, we can clearly observe square-wave is formed when $\theta = 90^\circ$ (Fig. 5a), At this angle, the $\lambda/2$ plate effectively rotates the TE and TM modes by 90° . The duration $\tau_2 = 5.4$ ns. The RF spectrum show the central peak is at 7.6 GHz. Increasing the angle to 150° results in a degradation of the square oscillations. The waveform broadens, indicating a loss of coherence in the TE mode as contributions from the TM mode become significant. The corresponding RF spectrum shows a decrease in intensity, with low-frequency components becoming more pronounced, reflecting the involvement of the TM mode in the dynamics. Further rotation to 240° leads to a further degradation of the oscillations, which manifest as small and wide pulses with minor oscillations superimposed. The RF spectrum associated with this configuration displays an even smaller intensity, indicating a considerable loss of coherence and a more complex interplay between the TE and TM modes.

Finally, we also study the spatial-temporal dynamics of the TE mode for the laser is operated at different pump currents. Fig. 6a-c are the dynamics within one round trip as a function of round-trip number, and Fig. 6a'-c' show the detail structure corresponding to the region within the orange square in Fig. 6a-c. At

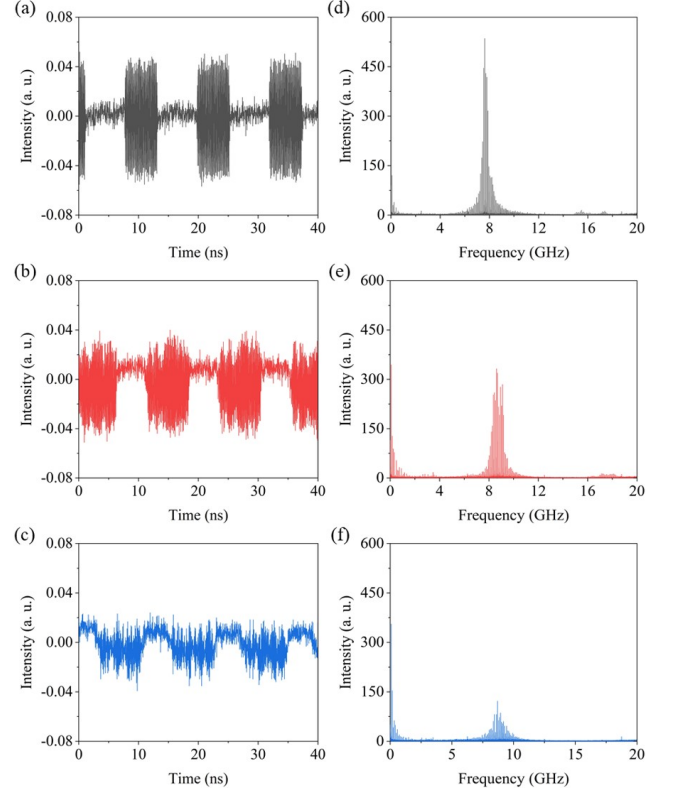


FIG. 5: Temporal dynamics and the corresponding RF spectra of the TE mode for different θ : (a) and (d), 90° ; (b) and (e), 150° ; (c) and (f) 240° .

a pump current of $2.64P_{th}^{TE}$, our analysis revealed fast oscillations that produced a distinct zigzag structure in the spatial-temporal domain (see Fig. 6a and a'). This pattern suggests that the fast oscillation is almost perfectly resonant with the feedback time but that its phase is still wandering in the course of many roundtrips. Increasing the pump current to $2.86P_{th}^{TE}$ resulted in a notable transition in the mode structure. A banded structure emerged, extending spatially and indicating the presence of square oscillations (Fig. 6b). Again, a stable (but non-stationary) pattern emerges, suggesting long-term coherence of the fast dynamics. Upon closer examination (Fig. 6b'), we observed defects within the pattern, in (4.2, 250) and (4.5, 460). We conjecture that these defects arise from the duration of the modulated phase not being an exact integer number of periods of the fast oscillation. Further increasing the pump current to $3.06P_{th}^{TE}$ led to the observation of an even broader banded structure (Fig. 6c). However, this higher level of feedback resulted in the formation of a larger number of defects near the left boundary indicating a degradation of coherence within temporal pattern of the TE mode. The details captured in Fig. 6c' reveal that these defects, which disrupt the previously observed coherent oscillations. Accordingly, the left and right

fronts on Fig. 6c are not strictly stationary with respect to each other.

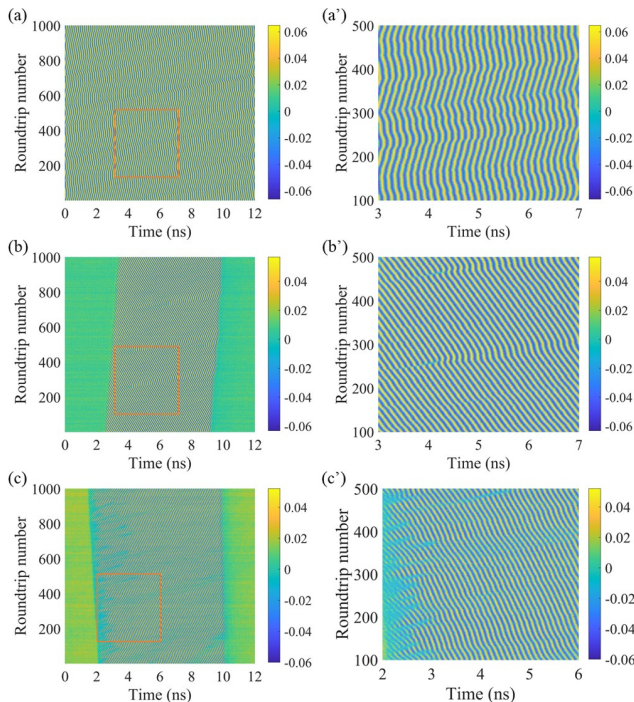


FIG. 6: Spatial-temporal dynamics of the TE mode for different pump currents: (a) and (a'), $2.64P_{th}^{TE}$; (b) and (b'), $2.86P_{th}^{TE}$; (c) and (c') $3.24P_{th}^{TE}$. (a')-(c') are the enlarge regions remarked in a-c.

CONCLUSIONS

In conclusion, we have successfully generated fast oscillations of the TE mode over a square wave polarization switching at a frequency different from the relaxation frequency and from the external-cavity frequency in a semiconductor VCSEL. Orthogonal polarization feedback induces a slow SW modulation of the laser polarizations and fast oscillations with possibly high modulation amplitude are observed on the upper state of the SW. Interestingly, although the polarization switching dynamics is induced by delayed optical feedback, that self-pulsation frequency does not scale with the time-delay. Instead, from free-running laser power spectra, we conjecture that this fast part of the dynamics is related to a resonance between the relaxation oscillation frequency of the TE mode and the laser birefringence. We have investigated the influence of the feedback level induced by the pump current, and the angle of the $\lambda/2$ plate, on the evolution of the dynamics of the TE mode. The results reveal that the resonance between the relaxation oscillation frequency of the TE mode and the longitudinal modes of the external

cavity has significant influence on the generation of the square fast oscillations. By plotting the spatial-temporal structure, we have identified some defects within the fast oscillation structure which we associate to near-resonance situation between the fast dynamics and the square wave polarization switching. Further analysis of the dynamics of the fronts in the spatiotemporal representation is left for future work. Our system shows a fairly simple system for the generation of square waves with tunable durations. This system could find applications in optical communications, and optical computing. In particular, the existence of fronts connecting oscillatory solution to a homogeneous solution may enable the formation of temporal localized states in a similar way to the front stabilization by oscillatory tails reported in [25].

Acknowledgment

The authors would like to thank Prof. Gang Xu for the insightful discussions. This work is partially supported by National Natural Science Foundation of China (Grant No. 61804036, and 62475206), Key Research and Development Plan of Shaanxi Province, China (Grant No. 2024GH-ZDXM-42), National Key Research and Development Program of China (Grant No. 2021YFB2801900, 2021YFB2801901, 2021YFB2801902, and 2021YFB2801904),

-
- [1] J. Tiana-Alsina and C. Masoller, "Dynamics of a semiconductor laser with feedback and modulation: experiments and model comparison," *Opt. Express*, 30, 9441-9449, (2022).
 - [2] T. Wang, C. Jiang, Q. Fang, X. Guo, Y. Zhang, C. Jin, S. Xiang, "Reservoir computing and task performing through using high- β lasers with delayed optical feedback," *Progress In Electromagnetics Research*, 178, 1-12, (2023).
 - [3] M. Skënderas, S. W. Jolly, and M. Virte, "Impact of feedback time-distribution on laser dynamics," *Phys. Rev. Res.* 6, 023025, (2024).
 - [4] J. G. Wu, Z. M. Wu, Y. R. Liu, L. Fan, X. Tang, and G. Q. Xia, "Simulation of bidirectional long-distance chaos communication performance in a novel fiber-optic chaos synchronization system," *J. Lightwave Technol.* 31, 461, (2013).
 - [5] C. Xue, N. Jiang, Y. Lv, C. Wang, G. Li, S. Lin, and K. Qiu, "Security-enhanced chaos communication with time-delay signature suppression and phase encryption," *Opt. Lett.* 41, 3690, (2016).
 - [6] A. Argyris, E. Pikasis, and D. Syvridis, Gb/s one-time-pad data encryption with synchronized chaos-based true random bit generators, *J. Lightwave Technol.* 34, 5325 (2016).
 - [7] P. Li, Y. Sun, X. Liu, X. Yi, J. Zhang, X. Guo, Y. Guo, and Y. Wang, "Fully photonics-based physical random bit generator," *Opt. Lett.* 41, 3347, (2016).

- [8] K. Myneni, S. D. Pethel, N. J. Corron, T. A. Barr, and B. R. Reed, "High precision ranging using a chaotic laser pulse train," *Appl. Phys. Lett.*, 78, 1496, 2001.
- [9] F. Y. Lin and J. M. Liu, "Chaotic radar using nonlinear laser dynamics," *IEEE J. Quantum Electron.*, 40, 815, (2004).
- [10] S. Xiang, S. Gao, Y. Shi, Y. Zhang, Z. Song, X. Guo, Y. Zhang, Y. Ma, and X. Chen, "Experimental demonstration of a photonic spiking neuron based on a DFB laser subject to side-mode optical pulse injection," 67, 132402, (2024).
- [11] T. Inagaki, K. Inaba, T. Leleu, T. Honjo, T. Ikuta, K. Enbutsu, T. Umeki, R. Kasahara, K. Aihara, and H. Takesue, "Collective and synchronous dynamics of photonic spiking neurons," *Nat. Commun.*, 12, 2325, (2021).
- [12] S. S. Li, X. Z. Li, J. P. Zhuang, G. Mezosi, M. Sorel, and S. C. Chan, "Square-wave oscillations in a semiconductor ring laser subject to counter-directional delayed mutual feedback," *Opt. Lett.*, 41, 812-815, (2016).
- [13] M. S. A. Mossaad, K. Su, W. Pawlikowski, Z. C. Zhang, S. Hranilovic and L. Lampe, "Square-wave spatial optical orthogonal frequency-division multiplexing," *IEEE Photonics Journal*, 16, 7301013, (2024).
- [14] A. Gavrielides, T. Erneux, D. Sukow, G. Burner, T. McLachlan, J. Miller, and J. Amonette, "Square-wave self-modulation in diode lasers with polarization-rotated optical feedback," *Opt. Lett.*, 13, 2006-2008, (2006).
- [15] A. Gavrielides, D. W. Sukow, G. Burner, T. McLachlan, J. Miller, and J. Amonette, "Simple and complex square waves in an edge-emitting diode laser with polarization-rotated optical feedback," *Phys. Rev. E*, 81, 056209, (2010).
- [16] D. Sukow, A. Gavrielides, T. Erneux, B. Mooneyham, K. Lee, J. McKay, and J. Davis, "Asymmetric square waves in mutually coupled semiconductor lasers with orthogonal optical injection," *Phys. Rev. E*, 81, 025206, (2010).
- [17] C. Masoller, D. Sukow, A. Gavrielides, and M. Sciamanna, "Bifurcation to square-wave switching in orthogonally delay-coupled semiconductor lasers: Theory and experiment," *Phys. Rev. A*, 84, 023838, (2011).
- [18] N. Yu, Q. J. Wang, C. Pflüg, L. Dieh, F. Capasso, T. Edamura, S. Furuta, M. Yamanishi, H. Kan, "Semiconductor lasers with integrated plasmonic polarizers," *Appl. Phys. Lett.*, 94, 151101, (2009).
- [19] A. Yariv and P. Yeh, "Photonics: optical electronics in modern communications," 6th ed. (Oxford University Press, Oxford), Chap. 16, p. 719., (2007).
- [20] G. Pan, M. Xun, X. Zhou, Y. Sun, Y. Dong, and D. Wu, "Harnessing the capabilities of VCSELs: unlocking the potential for advanced integrated photonic devices and systems," *Light Sci Appl*, 13, 229, (2024).
- [21] M. S. Islam, A. V. Kovalev, E. A. Viktorov, D. S. Citrin, and A. Locquet, "Optical square-wave generation in a semiconductor laser with optoelectronic feedback," *Opt. Lett.* 46, 6031-6034, (2021).
- [22] J. Mulet, M. Giudici, J. Javaloyes, and S. Balle, "Square-wave switching by crossed-polarization gain modulation in vertical-cavity semiconductor lasers," *Phys. Rev. A*, 76, 043801, (2007).
- [23] M. Marconi, J. Javaloyes, S. Barland, M. Giudici, and S. Balle, "Robust square-wave polarization switching in vertical-cavity surface-emitting lasers," *Phys. Rev. A*, 87, 013827, (2013).
- [24] C. H. Uy, L. Weicker, D. Rontani, M. Sciamanna, "Sustained oscillations accompanying polarization switching in laser dynamics," *Opt. Express*, 26, 16917-16924, (2018).
- [25] E. R. Koch, T. G. Seidel, S. V. Gurevich, and J. Javaloyes, "Square-wave generation in vertical external-cavity Kerr-Gires-Tournois interferometers," *Opt. Lett.*, 47, 4343-4346, (2022).
- [26] G. Friart, G. Verschaffelt, J. Danckaert, and T. Erneux, "All-optical controlled switching between time-periodic square waves in diode lasers with delayed feedback," *Opt. Lett.* 39, 6098-6101, (2014).
- [27] G. Giacomelli and A. Politi, "Relationship between delayed and spatially extended dynamical systems," *Phys. Rev. Lett.* 76, 2686, 1996.